Canadian Science Publishing
NRC Research Press journals | Publishing Services

Journal of Unmanned Vehicle Systems
Revue des systèmes de véhicules télécommandés

UAV magnetometry for chromite exploration in the Samail ophiolite sequence, Oman

Journal:	*Journal of Unmanned Vehicle Systems*
Manuscript ID	juvs-2017-0015.R2
Manuscript Type:	Article
Date Submitted by the Author:	17-Nov-2017
Complete List of Authors:	Parvar, Kiyavash; Queen's University, Geological Sciences and Geological Engineering; Pioneer Exploration Braun, Alexander; Queen's University, Geological Sciences and Geological Engineering Layton-Matthews, Daniel; Queen's University, Geological Sciences and Geological Engineering Burns, Michael; Pioneer Exploration
Keyword:	unmanned aerial vehicles, exploration geophysics, magnetometry, chromite exploration, magnetic gradiometry
Is the invited manuscript for consideration in a Special Issue? :	N/A

TITLE:

UAV magnetometry for chromite exploration in the Samail ophiolite sequence, Oman

Authors:

Kiyavash Parvar [1,2], Alexander Braun [1]*, Daniel Layton-Matthews [1], and Michael Burns [2]

[1] Department of Geological Sciences and Geological Engineering, Queen's University, Kingston, ON, Canada
[2] Pioneer Exploration, Saskatoon, SK, Canada
* Correspondence: braun@queensu.ca; Tel.: +1-613-533-6621

Abstract: Chromite occurrences in ophiolite complexes present valuable natural resources and require sophisticated geophysical exploration methods. As chromite does not exhibit significant geophysical anomalies, we propose an indirect method of detection by surveying for magnetic anomalies caused by the serpentinization of the chromite host rock, which contains magnetite developed through petrogenesis. An unmanned airborne vehicle (UAV) magnetometry test survey revealed a known chromite deposit. The results show that mapping for serpentinite is a viable option to find chromite provided the survey is conducted at low flight elevations (<60m above ground). The survey results reveal the location of a known chromite deposit and indicate that the magnetic susceptibility contrast between chromite and the surrounding serpentinite is low. It further indicates a low-grade serpentinization in the area, which requires very sensitive magnetometry surveys in close proximity to the targets provided by terrestrial and UAV platforms. The ability of UAV surveys to acquire observations of the magnetic field in 3-D enables the calculation of magnetic gradients, which show higher sensitivity compared to classical gradient estimation from 2-D observations.

Keywords: Unmanned aerial vehicles, airborne magnetometry, ophiolites, chromite deposits, magnetometry, mineral exploration, upward continuation, vertical magnetic gradient, exploration geophysics

1. Introduction

Magnetometry is a classical mineral exploration method (Hinze et al. 2013). Magnetometers can be deployed on satellite, airborne, sea-borne and terrestrial platforms. Recently, unmanned aerial vehicles (UAV) were used as platforms for magnetic surveys (Hashimoto et al. 2014; Parvar 2016; Cunningham 2016; Wood 2016). UAV magnetometry requires a careful consideration of payload integration, UAV magnetic impacts, and sensor orientation. In principle, multi-rotor UAV magnetometry, as employed herein, is able to fill an observational gap between airborne and terrestrial surveys. In addition, it allows for the acquisition of magnetic gradient measurements, which is rarely achieved via airborne and terrestrial surveys that are typically tied to 2-D survey grids (Hinze et al. 2013). UAVs enable flexible data acquisition in 3-D space and thus produce measured magnetic gradients, which allow for improved target characterization compared to total magnetic intensity (TMI) observations alone. In this study, we describe a magnetic survey conducted over chromite deposits in Oman as an example of initial exploration for magnetic anomalies. The primary emphasis is on the detectability of chromite deposits using UAV magnetometry and secondary is the relationship between chromite occurrences and the degree of serpentinization, which produces the magnetically susceptible host rocks. Magnetometry does not directly detect the low susceptibility of chromite, but rather the variations in susceptibility with respect to the surrounding serpentinite. The motivation for this study arises from the possibility of

increasing the detectability of chromite deposits leading to more discoveries through the use of a UAV survey, which can be conducted closer to the target compared to manned airborne surveys. This study does not attempt to characterize the geometry and susceptibility distribution of the chromite deposit, instead we focus on determining if chromite deposits are detectable with low-altitude UAV magnetometry.

The study area is located in the south-central region of the Samail Ophiolite sequence, Oman (Figure 1(a), Burg 2017; Rollinson et al. 2014). Obduction of the oceanic lithosphere onto the Arabian continental margin during the late-Cretaceous resulted in the formation of ophiolite complexes in Oman (Burg 2017; Rollinson et al. 2014; Searle and Cox 1999). In the Oman ophiolitic complexes, the following three types of chromite deposits are distinguishable according to their structural position (Auge 1987): i) Cumulate sequence deposits in the form of stratiform, ii) Top-mantle sequence deposits, iii) Deeper mantle deposits. Northern Oman exhibits numerous podiform chromite deposits within the peridotite complex overlain by gabbro (Peters and Kramers 1974). Deposits which are economically viable are in stratiform or tabular lenses (Ali and Jahangir Khan 2013). In Oman, the chromite deposits occur mainly in the mantle sequences of harzburgite and dunite (Ali and Jahangir Khan 2013). The mineral chromite is weakly paramagnetic and its magnetic susceptibility varies greatly in the range of 2×10^{-7} to 1.9×10^{-3} in SI units. However, in nature, chromite with this susceptibility range is uncommon and the expected range is 2×10^{-7} to 2.5×10^{-5} in SI units (Allen 2001).

Despite these measurements, chromite samples found in Omani ophiolites have shown larger susceptibility values which results in detectable targets in magnetic surveys (Ali and Jahangir Khan, 2013). Values of 3.1×10^{-4} to 3.7×10^{-4} in SI units are the measured values for the susceptibility of Omani chromite samples (Rais et al. 2012). Yungul (1956), Gunn (1997), and Wynn et al. (1984) were the first to identify a relationship between serpentinite concentrations and susceptibility of chromite samples. Hence, detecting serpentinite related to chromite deposits is the most probable exploration target for UAV magnetometry. Bonnemains et al. (2016) measured fifteen serpentinized peridotite samples across the Omani ophiolite complex and found a range of susceptibilities between 5×10^{-4} and 7.8×10^{-3} in SI units, which is approximately one order of magnitude larger than chromite.

The origin of chromite in partially serpentinized mantle rocks, such as the Oman ophiolites, has been the subject of continued debate (Roeder and Reynolds 1991; Matveev and Ballhaus 2002; Borisova et al. 2012). Most explanations invoke a basaltic genesis (e.g. Roeder and Reynolds, 1991; Python et al. 2008) with either a contribution from crustal contamination or melt mixing to place chromite on the liquidus. Others suggest a hybrid model of a magmatic system saturated with an aqueous fluid phase coupled with a physical separation of chromite from olivine under oxidizing conditions (Matveev and Ballhaus 2002; Feig et al. 2016). For the Oman chromitites there is a common consensus that an aqueous fluid was involved in the primary petrogenesis of chromite (Arai et al. 2006; Borisova et al. 2012). Secondary hydrothermal activity within the Oman ophiolites has been well-documented, ranging from high-temperature (~900 C) hydrothermal veining of anorthite and diopside (Python et al. 2008) to more classical low temperature assemblages of serpentine, chlorite, tremolite and magnetite (Abily et al. 2011).

This low temperature serpentinization of ultramafic rocks within ophiolites greatly influences their magnetic, gravity, and seismic properties (Dyment et al. 1997; Mevel 2003). Serpentinization within these types of rocks likely occurs as a two-step process. Initially at low temperatures (<250 C) pyroxene is relatively stable during hydrous alteration, and serpentine, magnetite, and brucite form (Bach et al. 2004). At either higher temperatures (>350 C), or higher water-rock interactions, complete serpentinization will result in the production of talc, tremolite and hematite (Allen and Seyfried 2003). Initially magmatitic chromites are mantled and progressively replaced by chromian

magnetite or magnetite. With prolonged serpentinization, chromite cores become progressively modified as a result of exchange of cations with surrounding minerals until only magnetite pseudomorphs remain (Frost 1985; Abzalov 1998; Barnes 2000). Consequently, the serpentinization process of the deposit controls if sufficient magnetic susceptibility allows for detection by UAV magnetometry.

The survey site is located 5 km east of Al Rawdha, a village approximately 90 km south of Muscat. It exhibits relatively flat terrain with topographic variations not exceeding ±5 metres across the approximately 600 m by 600 m area. Typical chromite mineralization in this region occurs at high elevations and is usually located near the contact of the lower cumulate sequence and mantle. The chromite mineralization is hosted by harzburgite and dunite. The characteristic geological features of the area consist of two major geological units shown in Figure 1(b):

I. Quaternary alluviums: These are mostly related to the sediments deposited by surface waters. These units (shown in yellow in Figure 1(b)) were carried and deposited along the wadi in the area.

II. Highly fractured ultramafic rocks. Most of these rocks are harzburgite-dunite units, which are a characteristic rock of Omani ophiolites (Auge 1987). Ultramafics are shown in orange color in Figure 1(b).

In addition to these two major units, serpentinization is evident along fractures with scattered occurrences throughout the survey site. The concentration of serpentinite is significantly higher closer to known chromite outcrops, which have been previously mined (Figure 2). However, detailed geological maps of the study site do not exist.

2. Methods and Materials

2.1 UAV Magnetometry System

Multicopters, also referred to as multi-rotor UAVs, are rotary wing UAVs. Energy loss from torque is minimized in multicopters because of the rotors rotating in opposite directions, however, reliance on electronic motors and batteries has limited efficiency of multicopters in comparison to single-rotor helicopters (Eck and Imbach 2011). Most recent multicopter models offer a payload of up to 5 kg and have the main advantages of operational ease, high flexibility and flight stability over other options (Siebert and Teizer 2014; Whitehead and Hugenholtz 2014). In order to conduct the field survey, a multi-rotor UAV-Mag™ system was employed, hereinafter referred to as UAV. The specifications of the platform are listed in Table 1.

The principal geophysical sensors in the UAV-Mag™ system include a GEM Systems GSMP-35A potassium vapour magnetometer, a Novatel OEMV1 multi-GNSS positioning system, an inertial measurement unit (IMU,) a laser altimeter, a multiplexor (MUX) data acquisition unit, and a UTC time synchronized base station GEM Systems GSM-19T magnetometer (GEM Systems 2016). The raw data stream of the GSMP-35A magnetometer is collected at a rate of 10 Hz, along with the auxiliary sensor data (IMU, GPS and laser altimeter), stored on-board the UAV, and retrieved post flight. The flight controller unit is a DJI A2 controller with flight programming and monitoring performed via a laptop or tablet ground station. The UAV-Mag™ system is shown in Figure 3. During a survey, the magnetometer sensor is suspended below the UAV platform at a distance of 3 metres. The magnitude of the UAV magnetic field is significantly larger than the magnetic signals of the targeted rocks, and thus must be eliminated through physical separation of the UAV and the magnetometer (Parvar 2016; Cunningham 2016). It was found that a separation distance of 3 metres ensures that the magnetic field components generated by the UAV and its motors are attenuated

sufficiently and approximate the noise level of airborne magnetic surveys. This distance was determined through a number of experiments described in the following section.

2.2 *Magnetic effects of the UAV*

To gain a better understanding of the magnetic field created by the UAV, and also to optimize the separation between the UAV and the GSMP-35A magnetometer, a laboratory survey was conducted. It should be noted that this experiment with a static UAV does not provide representative results for changes in yaw, pitch and roll due to operational UAV manoeuvres. A 3000 mm x 3000 mm grid was surveyed below the UAV suspended 3 metres above ground. A Honeywell HMR-2300 vector magnetometer was mounted on an adjustable pole, and positioned vertically at each of the survey points.

Measurements were taken with a horizontal grid spacing of 200 mm at 4 different elevations: 400, 800, 1200, 1600 mm below the UAV. The survey was conducted twice, with the UAV switched on and off resulting in 1024 individual measurements per survey. The data was interpolated onto a 3-D voxel grid using Kriging and spherical variograms in Geosoft Oasis Montaj 8.5. In Figure 4 the results obtained using a grid cell size of 40 mm and a blanking distance of 12 mm are shown.

The UAV (switched on) creates a dipole signal of approximately 350 nT at 400mm below the UAV which decays to approximately 9 nT at 1600 mm separation. Applying potential field theory with the aforementioned values, the following decay curve was generated (Figure 5). According to Figure 5, the magnetometer should be placed at distances further than 3000 mm in order to avoid unwanted UAV generated magnetic effects in excess of 1 nT. Effects of manoeuvres including changes in yaw, pitch and roll as well as the interactions of the UAV-generated magnetic field with the natural field must also be considered (Sterligov et al. 2016 and Versteeg et al. 2007). In Walter et al. (2017) the impact of yaw, roll and pitch on the magnetic data quality was studied with recommendations for limits of flight parameters to maintain airborne magnetic data standards. These experiments concluded that a similar separation of 3-4 metres is needed to avoid UAV magnetic effects at the magnetometer position.

2.3 *Field Survey in Oman*

In February 2016, Pioneer Exploration Consultants Ltd carried out magnetic surveys in order to determine the feasibility of UAV magnetometry for chromite detection. For validation purposes, a location with a known chromite outcrop was selected (red box in Figure 1b). As the terrain variability does not exceed ±5 metres, topographic effects on the TMI are considered negligible.

Based on geological surface observations, the estimated width of the chromite outcrop is less than 50 metres. Therefore, the survey lines were planned with a line spacing of 30 metres. In order to measure the vertical gradient, two 2-D surveys were conducted at elevations of 20m and 60m Above the Landing Zone (ALZ). The orientation of the survey lines was set to NE-SW perpendicular to the strike of the prevalent geological structures in the area (Figure 6). The selection of line spacing, survey area and length as well as the number of different elevations resulted from a compromise between logistical parameters and desired survey resolution. Logistical limitations in this remote area restricted the amount of acquired data. In order to cover both targets with minimal flight time, i) the known chromite deposit, and ii) a serpentinization area in the northern part of the site, the targets are located at the edge of the survey grid. While this is not best practise, as it could lead to edge effects in the calculation of gradients, this was a logistical requirement.

3. Results

3.1. Data Processing

The acquired data was processed using the following procedure (Parvar 2016); removing diurnal effects using base station observations and removing outliers. Outliers arise from loss of magnetometer lock, which is caused by sudden aircraft manoeuvres mostly at the end of the lines where directional acceleration is applied to the sensor. This causes the sensor to swing and rotate into the deadzone of the magnetometer (Walter et al. 2017). The data was interpolated onto a 2-D grid using via minimum curvature with an 8m cell size. The cell size was selected based on the dimensions of the target and the flight line spacing. A reduction to the pole was not applied because it does not provide more insight as the low-pass effect smoothens the signals from the chromite deposits and hinders localization. The interpolated TMI maps for the two flight elevations of 20m ALZ and 60m ALZ are shown in Figure 6. While the same flight path was programmed for both elevations, the actual path may differ by up to 1 metre based on an accuracy assessment of the onboard GNSS observations. Consequently, the data point distribution used for the interpolation is slightly different, but does not change the interpretation. To determine the noise level of the acquired data, the fourth difference method was applied (Coyle et al. 2014; Cunningham 2016). A histogram showing the distributions of the fourth difference values are shown in Figure 7.

The resulting interpolated grids illustrate that the anomaly related to the known chromite outcrop is detectable at 20m ALZ (TMI peak-top peak amplitude of 146 nT), but not at 60m ALZ. As the TMI decreases proportionally to the distance cubed, the signal of the chromite deposit is close to the noise level at 60m. In addition, this is an indication for:

I. a low susceptibility gradient between the chromite body and the host rock.

II. low-grade serpentinization.

Another anomaly can be identified in the north-central part of the survey area, which potentially shows the location of another highly serpentinized dunite. However, further drilling and trenching is suggested to confirm its presence.

3.2. 1st vertical gradient determination

In order to determine if the 1st vertical gradient of the magnetic data reveals more details about the chromite deposit, three different methods of gradient calculations were employed (Figure 8). This was done to determine the validity of each method and to evaluate the usefulness of acquiring TMI data at different elevations, instead of using upward continuation. The three methods are outlined below and result in 1st vertical gradients at 40m ALZ:

I. Calculating the 1st vertical gradient of the TMI by applying a vertical gradient filter. This process uses a Fourier Transform (FT) applied to the TMI values observed at 20m ALZ. The process results in the 1st vertical gradient at 20m. Applying an upward continuation filter of 20m to this gradient results in the 1st vertical gradient at 40m ALZ. We use the term "**Simple 1st vertical gradient**" for this method (green box). It should be noted that any upward continuation filter causes edge effects as a result of violating the requirement of having an infinite extent of observations.

II. Calculating the 1st vertical gradient of TMI data by subtracting upward continued values at 60m from the observed values at 20m ALZ. Dividing the differences by 40m results in the "**Average upward continued vertical gradient"** at 40m ALZ (blue box). Note that this upward continuation also suffers from edge effects.

III. Calculating the 1st vertical gradient of TMI by subtracting observed values at 60m from the observed values at 20m ALZ. The difference was divided by 40m elevation difference to obtain the **"Average observed vertical gradient"** at 40m ALZ (red box).

Note that methods II and III result in average gradients, which are calculated based on the average gradient between 20m and 60m. The average gradient is projected to an elevation of 40m, but does not necessarily represent the true gradient at 40m, due to the cubic decrease of the magnetic intensity with elevation. The term "average gradient" is commonly referred to gradients scaled by the distance between observations. Applying these three methods to the TMI data in Figure 6 results in the 1st vertical gradients shown in Figure 9. The **Simple 1st vertical gradient (Figure 9a)** represents the smallest amplitudes around the known outcrop, which makes it difficult to identify the outcrop without prior knowledge of its location. The **Average upward continued vertical gradient (Figure 9b)** is similar to the TMI at 20m (Figure 6(b)), and thus does not provide additional evidence. This is logical as the only information used in the gradient derivation originates from the TMI data at 20m ALZ. The **Average observed vertical gradient** shows a similar pattern but with higher amplitudes (0.56 nT/m higher) over the serpentinized area. Comparing the latter two reveals that upward continuation cannot replace a true observation, as the amount of information is limited to one flight elevation. The differences can thus lead to misinterpretation. While both show the location of the outcrop, the differences in the gradient magnitude are significant and require further attention. None of the gradients reveal more details about the position and geometry of the outcrop compared to the TMI data acquired at 20m ALZ. For future inverse modelling, the gradient (obtained from observations at two elevations) would better constrain the depth and geometry of the target, albeit not the focus of this study.

4. Conclusions

A UAV magnetometry survey was carried out at a known chromite outcrop in Oman. The survey results reveal the location of the known chromite deposit and potentially another deposit in magnetic observations (both TMI and vertical gradient) acquired at 20m ALZ. The anomalies are explained by serpentinite surrounding the chromite deposit. The grade of serpentinization determines the magnetic susceptibility and can be used as an indicator for chromite mineralization. However, the complexity of serpentinization and the resulting magnetic susceptibilities are not recoverable from magnetic observations alone. Due to the low susceptibilities of the rocks involved, a UAV or terrestrial survey is required to sense chromite deposits in this area. A UAV survey at 60m ALZ is not sensitive to localize the deposit rendering any manned aircraft surveys insensitive as well, as they operate above 60m above ground. UAV magnetometry enables exploration for chromite deposits through closer proximity to the targets as well as the ability to conduct magnetic surveys in 3-D and therefore fills an observational gap between terrestrial and manned airborne surveys.

Acknowledgments: Scholarships provided to K.P. by the Society of Exploration Geophysicists (SEG) and the American Association of Petroleum Geologists (AAPG) are greatly acknowledged. Funding for this study was provided by a Queen's University Research Initiation Grant to A.B.

References

Abily, B., Ceuleneer, G., and Launeau, P. 2011. Synmagmatic normal faulting in the lower crust: Evidence from the Oman ophiolite. Geology, **39**, pp 391-394

Abzalov, M. Z. 1998. Chrome-spinels in gabbro–wehrlite intrusions of the Pechenga area, Kola Peninsula, Russia: emphasis on alteration features. Lithos, **43**, pp 109–134

Ali, M. and Jahangir Khan, M. 2013. Geophysical Hunt for Chromite in Ophiolite. International Journal of Economic and Environmental Geology, **4**(2), pp 22-28

Allen, D. E., and Seyfried, W. E. 2003. Compositional controls on vent fluids from ultramafic-hosted hydrothermal systems at mid-ocean ridges: An experimental study at 400°C, 500 bars. Geochimica et Cosmochimica Acta, **67**, 1531-1542

Allen, N.R. 2001. The concept of magnetic mineral separation by particle rotation. Magnetic and Electrical Separation, Vol. **11**, No. 1-2, pp 33-50

Arai, S., Kadoshima, K., and Morishita, T. 2006. Widespread arc-related melting in mantle section of the northern Oman ophio- lite as inferred from detrital chromian spinels. Journal of the Geological Society, London, **163**, pp 1-11

Auge, T. 1987. Chromite deposits in the northern Oman ophiolite: mineralogical constraints. Mineralium Deposita, **22**, 1-10

Bach, W., Garrido, C.J., Paulick, H., Harvey, J., and Rosner, M. 2004. Seawater-peridotite interactions: First insights from ODP Leg 209, MAR 15°N. Geochemistry Geophysics Geosystems, **5**, Q09F26, doi:10.1029/2004GC000744

Barnes, S.J. 2000. Chromite in komatiites, II. Modification during greenschist to mid-amphibolite facies metamorphism. Journal of Petrology, **41**(3), pp.387-409

Bonnemains, D., Carlut, J., Escartin, J., Mével, C., Andreani, M., and Debret, B. 2016. Magnetic signatures of serpentinization at ophiolite complexes. Geochemistry Geophysics Geosystems, 17, 2969–2986, doi:10.1002/2016GC006321.

Borisova, A.Y., Ceuleneer, G., Kamenetsky, V.S., Arai, S., Béjina, F., Abily, B., Bindeman, I.N., Polvé, M., De Parseval, P., Aigouy, T., and Pokrovski, G.S. 2012. A new view on the petrogenesis of the Oman ophiolite chromitites from microanalyses of chromite-hosted inclusions. Journal of Petrology, **53**(12), pp 2411-2440

Burg, J.P. 2017. Oman: An Obduction Orogen. Structural Geology and Tectonics. ETH Zürich and Universität Zürich. Geologisches Institut, available online: http://www.files.ethz.ch/structuralgeology/JPB/files/English/Omaneng.pdf , accessed [March 1, 2017]

Coyle, M., Dumont, R., Keating, P., Kiss, F., and Miles, W. 2014. Geological Survey of Canada Aeromagnetic Surveys: Design, Quality Assurance, and Data Dissemination. Geological Survey of Canada Open File 7.

Cunningham, M. 2016. Aeromagnetic surveying with unmanned aircraft systems. MSc thesis, Carleton University. Ottawa, Ontario, Canada

Dyment, J., Arkani-Hamed, J., and Ghods, A. 1997. Contribution of serpentinized ultramafics to marine magnetic anomalies at slow and intermediate spreading centres: Insights from the shape of the anomalies. Geophysical Journal International, 129, pp 691– 701

Eck, C., and Imbach, B. 2011. Aerial Magnetic Sensing With an UAV Helicopter. International Archives of the Photogrammetry, Remote Sensing and Spatial Information Sciences, Vol. XXXVIII-1/C22. UAV-g 2011, Conference on Unmanned Aerial Vehicle in Geomatics, Zurich, Switzerland

Feig, S.T., Koepke, J., and Snow, J. E. 2016. Effect of water on tholeiitic basalt phase equilibria: an experimental study under oxidizing conditions. Contributions to Mineralogy and Petrology, **152**, pp 611-638

Frost, B.R. 1985. On the stability of sulfides, oxides and native metals in serpentinite. Journal of Petrology, **26**, pp 31–63

GEM Systems 2016. UAV Solutions Fixed-wing, Multicopter and Rotary-wing platforms featuring ultra-light Potassium Magnetometer. GEM Systems brochure for newly developed GSM-35U. A potassium magnetometer developed for UAVs. http://www.gemsys.ca/wp-content/themes/gemsystems/pdf/GEM_UAV_Solutions-GSMP_35U.pdf?lbisphpreq=1 , accessed [Nov 20, 2017]

Gunn, P.J., and Dentith, M.E. 1997. Magnetic responses associated with mineral deposits. AGSO Journal of Australian Geology & Geophysics, **17**(2), 145-158

Hashimoto, T., Koyama, T., Kaneko, T., Ohminato, T., Yanagisawa, T., Yoshimoto, M., and Suzuki, E. 2014. Aeromagnetic survey using an unmanned autonomous helicopter over Tarumae Volcano, northern Japan. Exploration Geophysics, 45, pp 37–42

Hinze, W.J., Von Frese R.R.B., and Saad, A.H. 2013. Gravity and Magnetic Exploration, Cambridge University Press

Matveev, S., and Ballhaus, C. 2002. Role of water in the origin of podi- form chromitite deposits. Earth and Planetary Science Letters, **203**, 235-243

Mevel, C. 2003. Serpentinization of abyssal peridotite at mid-ocean ridges. Comptes Rendus Geoscience, **335**, pp 825–852

Parvar, K. 2016. Development and evaluation of unmanned aerial vehicle (UAV) magnetometry systems. MASc thesis, Queen's University, Kingston, ON, Canada

Peters, T.J., and Kramers, J.D. 1974. Chromite Deposits in the Ophiolite Complex of Northern Oman. Mineralium Deposita, **9**, pp 253-259

Python, M., Ceuleneer, G., and Arai, S. 2008. Cr-spinel in mafic-ultramafic mantle dykes: evidence for a two-stage melt production during the evolution of the Oman ophiolite. Lithos, **106**, pp 137-154

Rais, A., Yousif, A.A., Worthing, M.A., and A1-Alawi, Z. 1997. Magnetic susceptibilities of chromites from Oman. Mineralogical Magazine, Vol. **61**, pp 726-728

Roeder, P.L., and Reynolds, I. 1991. Crystallization of chromite and chromium solubility in basaltic melts. Journal of Petrology, **32**, pp 909–934

Rollinson H.R., Searle M.P., Abbasi I.A., Al-Lazki A., and Al Kindi, M.H. 2014. Tectonic evolution of the Oman Mountains. Geological Society Special Publication, London, 392, 471 p

Searle, M., and Cox, J. 1999. Tectonic setting, origin, and obduction of the Oman ophiolite. Geological Society of America Bulletin, **111** (1), pp 104-122

Siebert, S., and Teizer, J. 2014. Mobile 3D mapping for surveying earthwork projects using an Unmanned Aerial Vehicle (UAV) system. Automation in Construction, **41**, pp 1–14

Sterligov, B., and Cherkasov, S. 2016. Reducing Magnetic Noise of an Unmanned Aerial Vehicle for High-Quality Magnetic Surveys. International Journal of Geophysics, Volume 2016, doi:10.1155/2016/4098275

Versteeg, R., McKay, M., Matt, A., Johnson, R., Selfridge, B., and Bennett, J. 2007. Feasibility study for an Autonomous UAV -Magnetometer system. Idaho National Laboratory, Idaho Falls, ID, 83415, November 2007

Walter, C., Braun, A., and Fotopoulos, G. 2017. Integrating a Potassium Vapour UAV Magnetometer with a Multi-Rotor UAV Towards Industry Standard Airborne 3D Magnetic Gradiometry. Canadian Exploration Geophysical Society (KEGS) Symposium, Innovation and New Methods in Geophysics, Toronto, March 4th, 2017. Extended abstract, 3pp.

Whitehead, K., and Hugenholtz, C. H. 2014. Remote sensing of the environment with small unmanned aircraft systems (UASs), part 1: a review of progress and challenge. Journal of Unmanned Vehicle Systems, **02**:69-85, 10.1139/juvs-2014-0006

Wood, A., Cook, I., Doyle, B., Cunningham, M., and Samson, C. 2016. Experimental aeromagnetic survey using an unmanned air system. The Leading Edge, **35**(3): 270-273; doi: 10.1190/tle35030270.1.

Wynn, J.C., and Hasbrouck, W.P. 1984. Geological and Geophysical Studies of Chromite Deposits in the Josephine Peridotite, Northwestern California and Southwestern Oregon. A Magnetic Interpretation of the Josephine Peridotite, Del Norte County, California. U.S. Geological Survey Bulletin, 1546-D

Yungul, S. 1956. Prospecting for chromite with gravimeter and magnetometer over rugged topography in east Turkey. Geophysics, **21**, 433-454.

FIGURE CAPTIONS:

Figure 1: (**a**) Study area in Oman indicated by red star, located ~90km southwest of Muscat. Background shows GTOPO30 Digital Elevation Model. (**b**) An illustration of the test site including locations of major geological units based on field observations. Quaternary – yellow; Ultramafic – orange; Serpentinite – blue; known Chromite outcrops - black. The star denotes the take-off and landing site.

Figure 2: Serpentinization at the known chromite outcrop in the study area (shown with black color in Figure 1b).

Figure 3: UAV-Mag™ system with a GEM Systems GSMP-35A magnetometer suspended 3 metres below.

Figure 4: A cross section of the 3D interpolated field based on the difference between the magnetic measurements of the UAV switched on and off. An impact as high as 350 nT is found at 400 mm below the UAV, but decays to 9 nT at a level of 1600 mm below the UAV.

Figure 5: Remaining UAV generated magnetic signal with increasing separation from the magnetometer. The UAV magnetic effect decays to 1 nT for a separation of 3300 mm. Curve based on measurements up to 1600 mm separation and potential field theory for larger separation.

Figure 6: (**a**) Acquired, filtered and interpolated total magnetic intensity (TMI) data at 60m Above Landing Zone (ALZ). Lines represent the approximate UAV flight path. (**b**) TMI data at 20m ALZ. Known chromite outcrop is shown by a small ellipse. The larger ellipse indicates a potential second deposit that does not exhibit a visible outcrop. Note that the known chromite outcrop is not visible in the data collected at 60m ALZ.

Figure 7: Histograms of the fourth difference data collected at 20m (top) and 60m (bottom) ALZ. Dotted vertical lines at ±0.05 nT represent the lower and upper limits of industry standard quality for fourth difference airborne magnetic observations (Coyle 2014).

Figure 8: Processing scheme employed in this study to derive three different 1st vertical gradients of the magnetic field.

Figure 9: 1st vertical gradient of the observed and upward continued TMI data at 40m ALZ. a) Simple 1st vertical gradient (I), b) Average upward continued vertical gradient (II), c) Average observed vertical gradient (III).

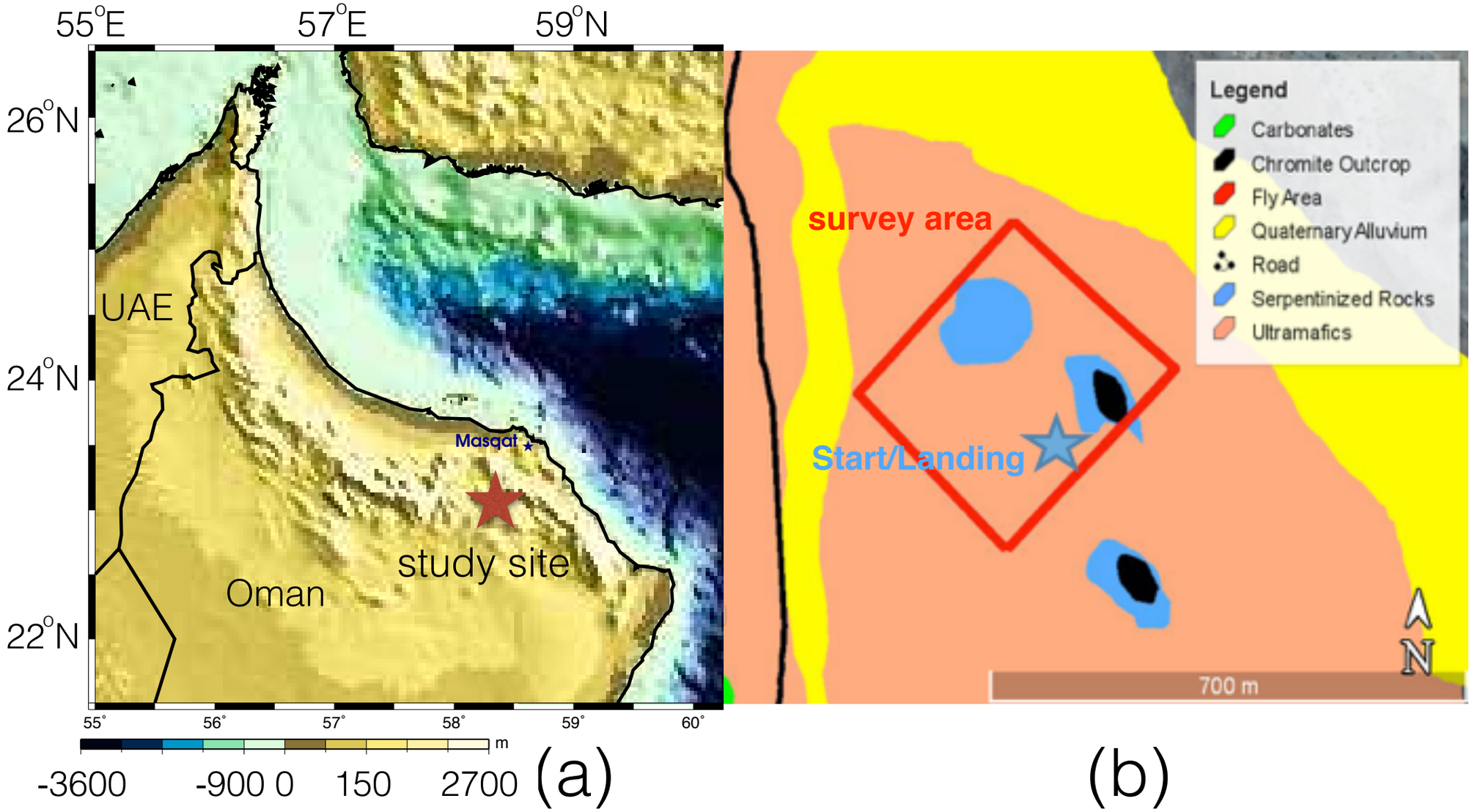
55°E
57°E
59°N
26°N
24°N
22°N
UAE
Masqat
study site
Oman
55°
56°
57°
58°
59°
60°
m
-3600
-900 0
150
2700
(a)
survey area
Start/Landing
Legend
Carbonates
Chromite Outcrop
Fly Area
Quaternary Alluvium
Road
Serpentinized Rocks
Ultramafics
N
700 m
(b)

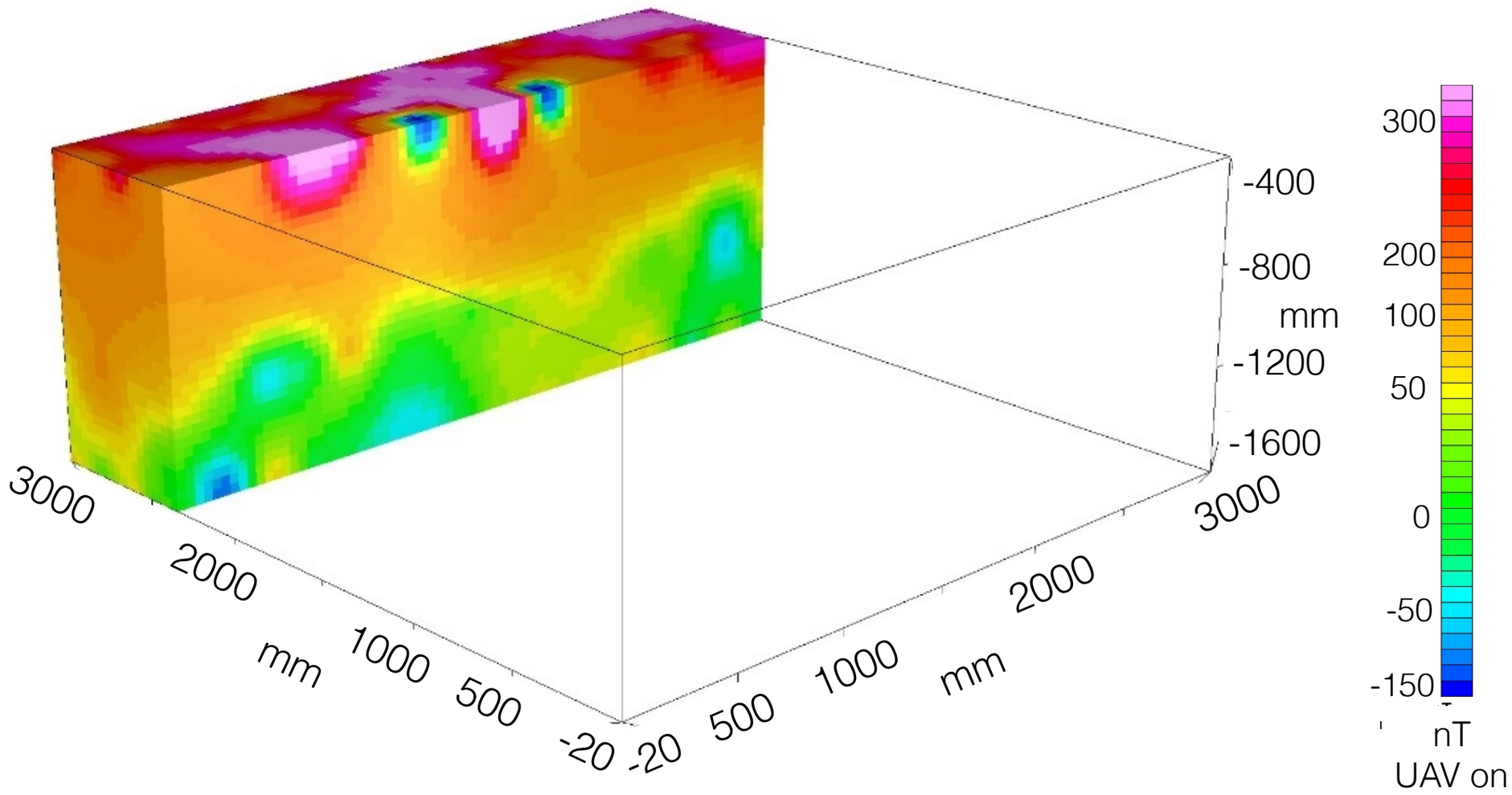
-400
-800
mm
-1200
-1600
3000
2000
1000
500
-20
3000
2000
1000
500
-20
mm
300
200
100
50
0
-50
-150
nT
UAV on

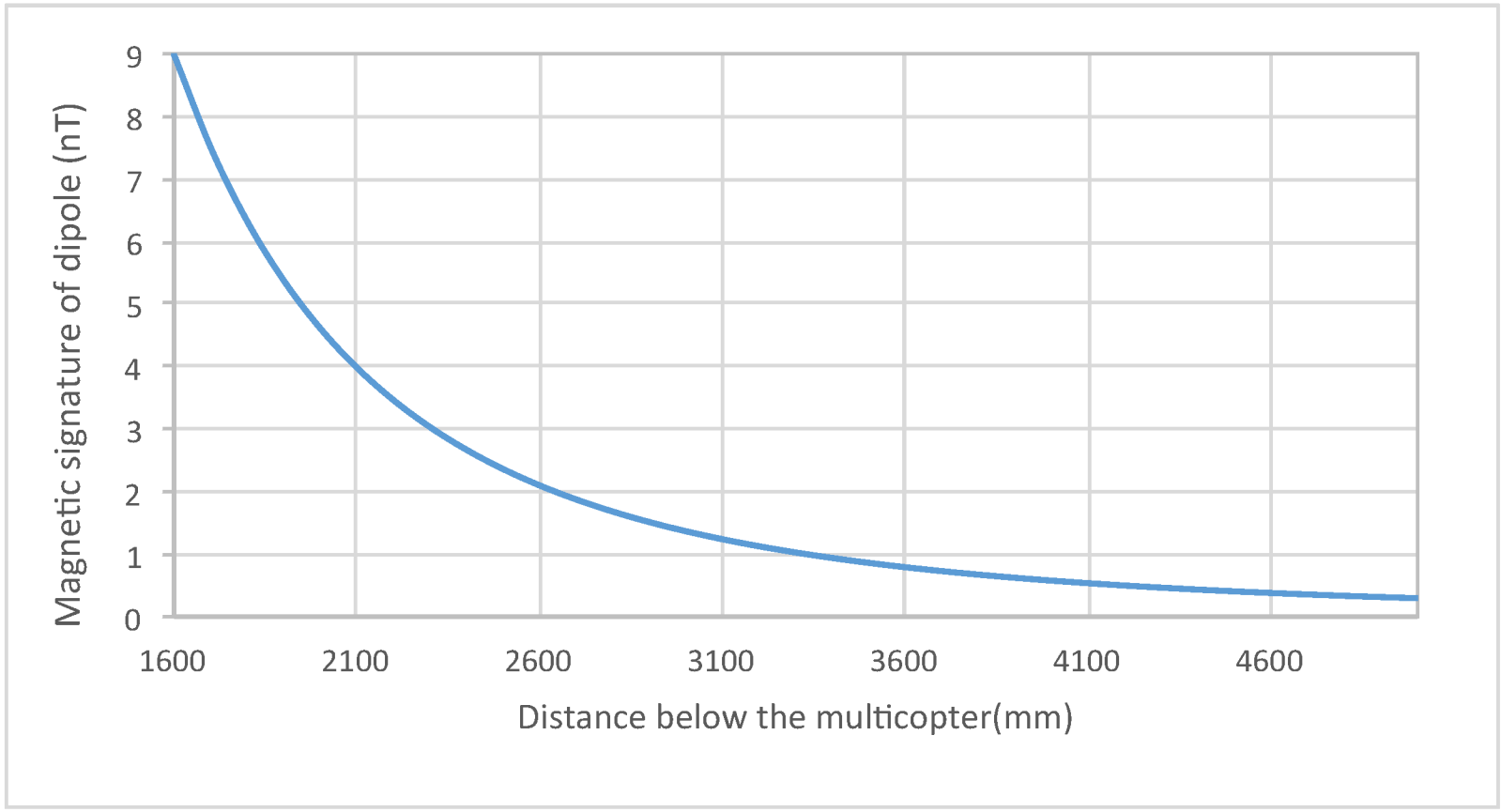
Magnetic signature of dipole (nT)
9
8
7
6
5
4
3
2
1
0
1600
2100
2600
3100
3600
4100
4600
Distance below the multicopter(mm)

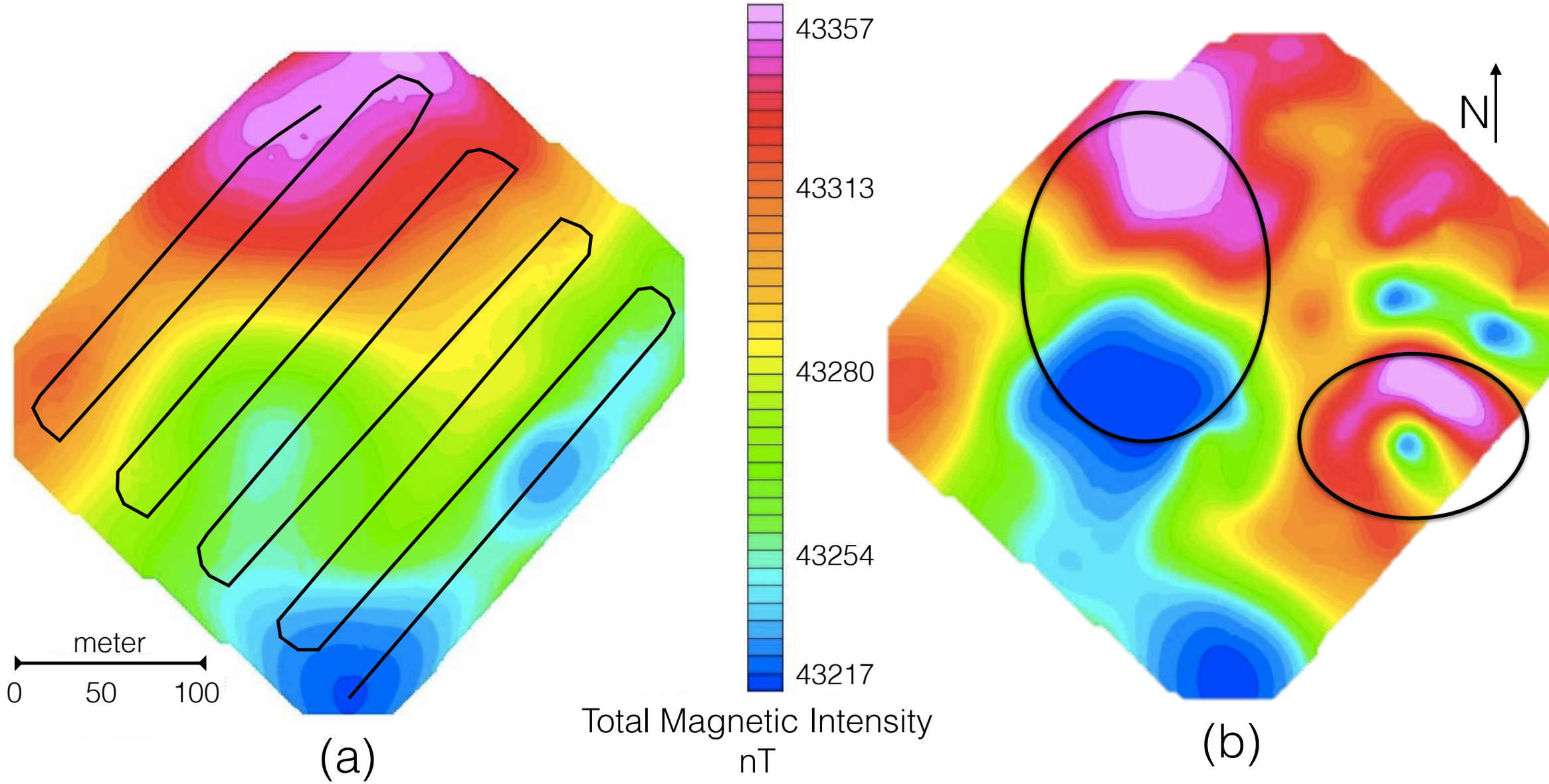
43357
43313
43280
43254
43217
Total Magnetic Intensity
nT
N
meter
0
50
100
(a)
(b)

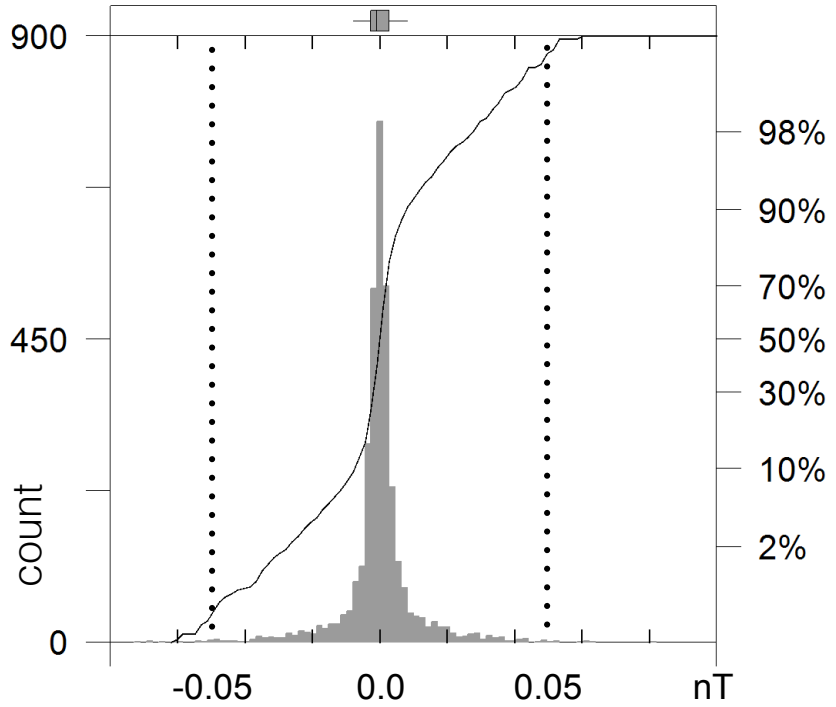

Fourth difference 20 metres ALZ

Samples:	3395
Minimum:	-0.07
Maximum:	0.08
Mean:	0.00
Geo.Mean:	0.00
Median:	-9.09e-013
Mode:	0.00
Std.Dev.:	0.01051
Std.Err.:	0.0001804
Skew:	-0.1316
Kurtosis:	10.07

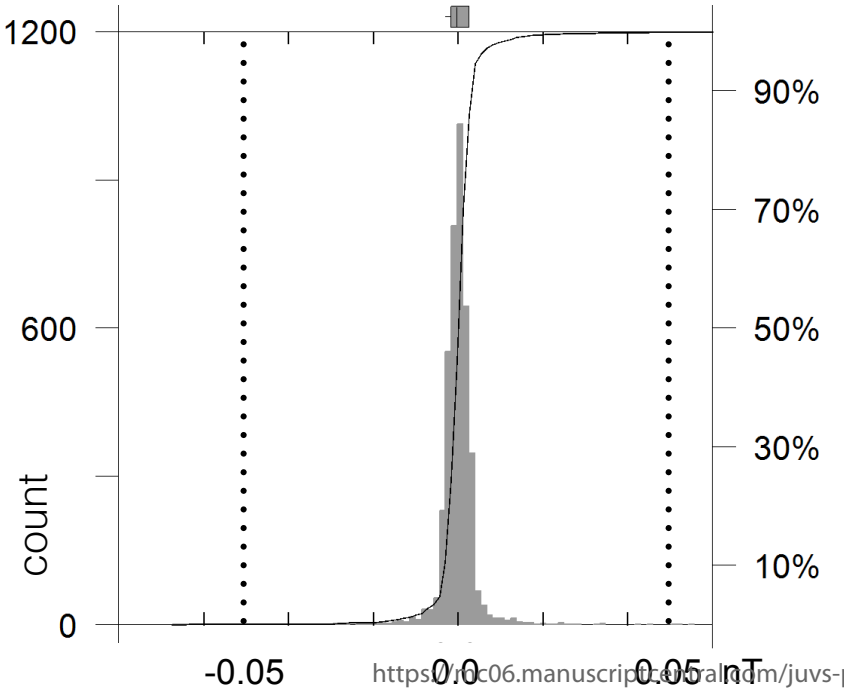

Fourth difference 60 metres ALZ

Samples:	4006
Minimum:	-0.07
Maximum:	0.05
Mean:	0.00
Geo.Mean:	0.00
Median:	-9.09e-013
Mode:	-4.55e-013
Std.Dev.:	0.004749
Std.Err.:	0.00007503
Skew:	-0.6308
Kurtosis:	51.04

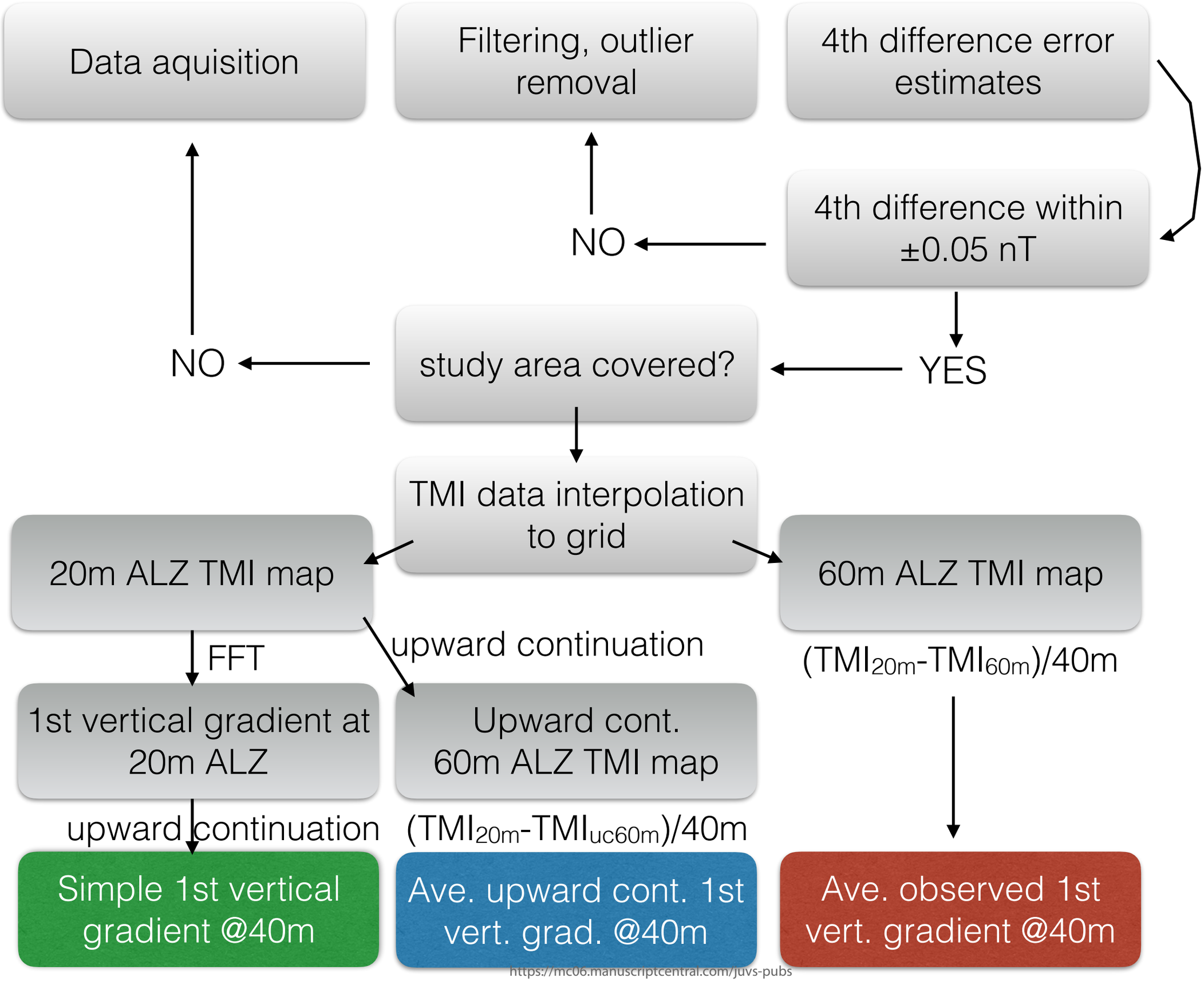
Data aquisition
Filtering, outlier removal
4th difference error estimates
4th difference within ±0.05 nT
NO
NO
study area covered?
YES
TMI data interpolation to grid
20m ALZ TMI map
60m ALZ TMI map
FFT
upward continuation
(TMI20m-TMI60m)/40m
1st vertical gradient at 20m ALZ
Upward cont. 60m ALZ TMI map
upward continuation
(TMI20m-TMIuc60m)/40m
Simple 1st vertical gradient @40m
Ave. upward cont. 1st vert. grad. @40m
Ave. observed 1st vert. gradient @40m

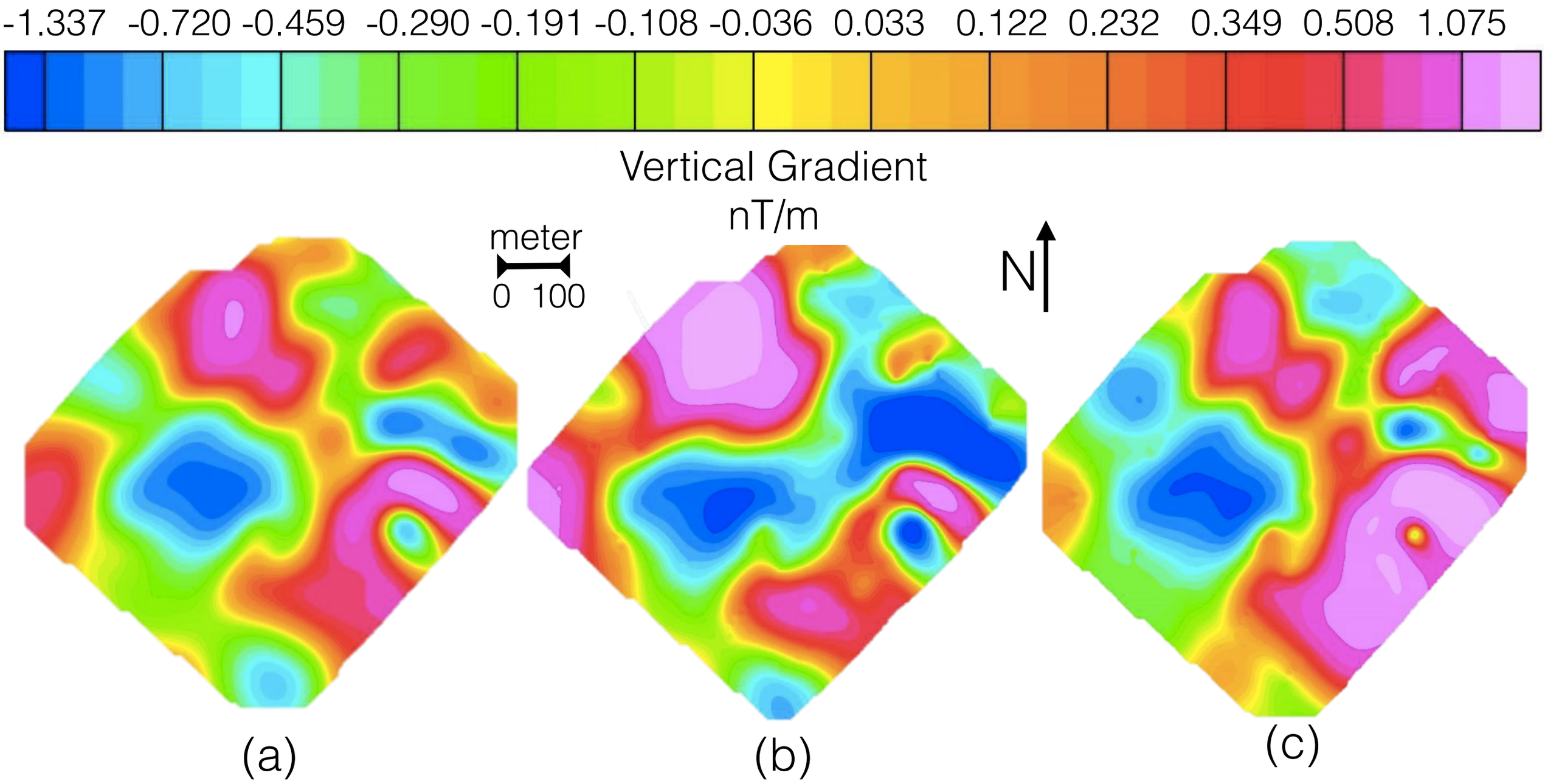
-1.337 -0.720 -0.459 -0.290 -0.191 -0.108 -0.036 0.033 0.122 0.232 0.349 0.508 1.075
Vertical Gradient
nT/m
meter
0 100
N
(a)
(b)
(c)

Table 1: Specifications of the UAV platform used in the UAV- Mag™ system.

Overall Width	121.9 cm
Number of motors (1 rotor each)	6
Fixed pitch	14.7 cm
Max current at max thrust	37 Ampere
Max lift capacity	14.4 kg
Thrust per motor	1.5 kg
Battery capacity	2 x 11,000 mAh batteries = 22,000 mAh
Battery weight	2.5 kg
Typical take-off weight	7.9 kg